2020 IEEE/RSJ International Conference on Intelligent Robots and Systems (IROS)
October 25-29, 2020, Las Vegas, NV, USA (Virtual)

Improving Disturbance Rejection and Dynamics of Cable Driven Parallel Robots with On-board Propellers

Imane Khayour, Loïc Cuvillon, Côme Butin, Arda Yiğit, Sylvain Durand, Jacques Gangloff
ICube Laboratory, Strasbourg University, INSA Strasbourg, UMR CNRS 7357, Strasbourg, France
Emails: come.butin@gmail.com, {khayour, l.cuvillon, arda.yigit, sdurand, jacques.gangloff}@unistra.fr

***Abstract*— This work studies redundant actuation for both trajectory tracking and disturbance rejection on flexible cable-driven parallel robots (CDPR). High dynamics/bandwidth unidirectional force generators, like air propellers, are used in combination with conventional but slower cable winding winches. To optimally balance the action of the two types of actuation within their saturation constraints, a model predictive controller is used. Experiments show the added value of on-board propulsion units with respect to winch-only control in order to improve the overall CDPR dynamic behavior.**

I. Introduction

Cable-Driven Parallel Robots (CDPRs) exhibit some advantages compared to rigid-link robots. They can cover a much larger workspace with higher dynamics due to lower link inertia. They are also cost-effective, easily scalable and may handle heavy payloads [1]. However, a low stiffness of the cables can impair the CDPR dynamics:

- the settling time of the end effector is longer due to slowly damped low-frequency oscillations of the platform;
- the large force bandwidth of the winch actuators is reduced due to the actuator speed saturation [2]: the lower the cable stiffness is, the longer the cable length to wind for a desired force on the end effector is (Hooke's law).

It is especially true for manipulators using very long cables or light cables made of a flexible material like polymers. These types of CDPRs may be used for tasks on high buildings (window cleaning, wall painting, etc.) [3] or to move a broadcast camera over a stadium [4].

Several strategies have been proposed to actively cancel the vibrations using the torque [5] or position controlled CDPR winches [6], [7]. To further improve the rejection of disturbances and vibrations, additional actuators have been mounted on the end effector. Inertia-based actuators like reaction wheels [8] or pendulum actuators [9]–[11] have been tested. However, these inertia-based actuators modify the end-effector inertia and can only generate a transient wrench (force and torque) before reaching their maximum velocity. To overcome some of these limitations, we propose to use unidirectional thrusters or force generators, such as cold-gas thrusters or air propellers. Both have short response time and can generate a continuous wrench. These types of actuators have been studied in a previous work [12] and have proved to be efficient for active damping of a suspended CDPR.

In this paper, the association of winches and on-board air propellers is used to reject disturbances and to track a reference trajectory on a CDPR. When long and/or elastic cables are used, the aforementioned large force bandwidth of the winch is reduced due to the actuator speed limit, impairing the bandwidth of the winch-only actuated CDPR position control loop. The addition of fast on-board propellers can solve this issue and improve trajectory tracking as well as disturbance rejection performance. Note that the propeller force can also be used to increase the downward acceleration of a suspended CDPR. Indeed, since there is no antagonist cable between the end effector and the ground, the downward acceleration of such robot is limited by the gravity.

Distributing the desired wrench on the CDPR end effector over the redundant winch and propeller actuators is known as control allocation. Control allocation has been extensively studied [13] on air/spacecrafts, ships, underwater [14] or electric vehicles. Among the proposed algorithms, Model Predictive Control Allocation (MPCA) has been proposed in [15] to take into account the saturation constraints of the actuators as well as their dynamics. More recently in [16], a Model Predictive Controller (MPC) that simultaneously computes the required wrench to track a trajectory and allocates this wrench to redundant actuators has been studied.

This work is a preliminary study evaluating this last control strategy applied to CDPR with fast response on-board force generators. A constrained MPC [17] is designed within a visual servo loop to explicitly handle the tracking of a reference trajectory, the rejection of disturbances and the actuator saturation in the control allocation. The control performance is evaluated experimentally on a planar suspended CDPR with four propellers mounted on the end effector and driven by DC brushless motors.

The remainder of the paper is organized as follows. Section II describes the system and dynamic equations of a CDPR with on-board actuators. Section III introduces the robot prototype and the experimental setup. The MPC controller design and the experimental results are presented in Section IV.

II. System Description

A CDPR with a number n_τ of cables and n_t of on-board unidirectional force generators (UFG) is considered (Fig. 1), such that the actuation is redundant : $n_\tau + n_t > n$, with n the degrees of freedom (DoF).

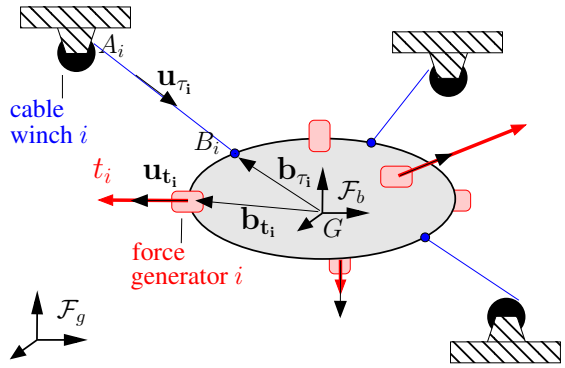

Fig. 1: Cable driven parallel robot with on-board actuators.

Let $\mathbf{x} = [\mathbf{p}^T, \boldsymbol{\theta}^T]^T \in \mathbb{R}^n$ be the pose of the CDPR end effector in the inertial frame $\mathcal{F}_g$, with $\mathbf{p}$ the vector of coordinates of its center of gravity G and $\boldsymbol{\theta}$ the vector of Euler angles describing its orientation.

A. Winch Actuator

A cable is modeled as a linear spring with negligible mass. If the cable is under tension, its geometry is a straight line between its attachment points (Fig. 1) and the cable length is l_1. The axial stiffness k of a cable is defined by $k = k_s/l_2$, where k_s is the specific stiffness and l_2 is the cable free length, i.e. the cable length when its tension is equal to zero. Unwinding the cable increases its free length, and thus decreases its stiffness.

The winch actuators are rotary motors that wind cables around winch spools to adjust the cable free length vector $\mathbf{l_2} = [l_{21}, \dots, l_{2n_\tau}]^T$. Assuming a null tension of the cable stored in the winch spool, the free lengths $\mathbf{l_2}$ are linked to the angular positions $\boldsymbol{\alpha}$ of the winch motor by the radius of the winch spool r: $\mathbf{l_2} = r\,\boldsymbol{\alpha}$.

The winch motors are assumed to be controlled by low-level velocity loops with a velocity reference $\dot{\mathbf{l}}_2^*$ as control input. Their dynamics can then be considered decoupled from the end-effector dynamics due to the high gain of the velocity loop [6]. However, the maximum velocity $\dot{l}_{2max}$ of an actuator is limited. The winch actuator dynamics are modeled as a second order system of natural frequency ω_n and damping ratio ξ:

$$\dddot{\mathbf{l}}_2 + 2\xi\omega_n \ddot{\mathbf{l}}_2 + \omega_n^2 \dot{\mathbf{l}}_2 = \omega_n^2 \dot{\mathbf{l}}_2^* \tag{1}$$

with the input constraints $-\dot{l}_{2max} \leq \dot{l}_{2_i}^* \leq \dot{l}_{2max}$.

Moreover, as the cables can pull but not push, the tension vector $\boldsymbol{\tau} \in \mathbb{R}^{n_\tau}$ is a vector of scalar tensions $\tau_i > 0$. This tension vector is given by:

$$\boldsymbol{\tau} = \mathbf{K}_\tau(\mathbf{l_2})[\mathbf{l_1}(\mathbf{x}) - \mathbf{l_2}] \tag{2}$$

with $\mathbf{K}_\tau = \mathrm{diag}(k_1, \dots, k_{n_\tau})$, the diagonal matrix of cable stiffness and $(\mathbf{l_1} - \mathbf{l_2})$ the vector of cable elongations. The wrench matrix $\mathbf{W}_\tau \in \mathbb{R}^{n \times n_\tau}$ maps the cable tensions $\boldsymbol{\tau}$ to the force $\mathbf{F}_\tau$ and moment $\mathbf{N}_\tau$ applied to the end effector [18]:

$$\begin{bmatrix} {}^g\mathbf{F}_\tau \\ {}^g\mathbf{N}_\tau \end{bmatrix} = -\underbrace{\begin{bmatrix} {}^g\mathbf{u}_{\tau\mathbf{1}} & \dots & {}^g\mathbf{u}_{\tau\mathbf{n}_\tau} \\ {}^g\mathbf{b}_{\tau\mathbf{1}} \times {}^g\mathbf{u}_{\tau\mathbf{1}} & \dots & {}^g\mathbf{b}_{\tau\mathbf{n}_\tau} \times {}^g\mathbf{u}_{\tau\mathbf{n}_\tau} \end{bmatrix}}_{\mathbf{W}_\tau(\mathbf{x})} \boldsymbol{\tau} \tag{3}$$

with ${}^g\mathbf{u}_{\tau_i}$ the coordinates in $\mathcal{F}_g$ of the ith cable unit direction vector and ${}^g\mathbf{b}_{\tau_i}$ the coordinates of the vector between G and B_i, the cable attachment point (see Fig. 1).

B. Unidirectional Force Generators

To enhance the dynamic behavior of the CDPR, additional unidirectional force generators (UFGs) are embedded in the end effector. Cold-gas thrusters or air propellers are some of the actuators candidates.

The UFGs are selected to have a high bandwidth while producing a unidirectional thrust $t > 0$ up to a saturation value t_{max}. Let $\mathbf{t} = [t_1, \dots, t_{n_t}]^T$ be the vector of the UFGs thrusts. The UFG actuators are modeled as first order dynamic systems with a time constant T_t between their control inputs $\mathbf{t}^*$ and thrust outputs $\mathbf{t}$:

$$T_t\,\dot{\mathbf{t}} + \mathbf{t} = \mathbf{t}^* \tag{4}$$

with the input constraints $0 \leq t_{min} \leq t_i^* \leq t_{max}$.

The thrust direction vector $\mathbf{u_{t_i}}$ is constant within the end-effector body frame $\mathcal{F}_b$ as depicted in Fig. 1. Thereby, the resulting wrench on the end effector is given by:

$$\begin{bmatrix} {}^b\mathbf{F_t} \\ {}^b\mathbf{N_t} \end{bmatrix} = -\underbrace{\begin{bmatrix} {}^b\mathbf{u_{t1}} & \dots & {}^b\mathbf{u_{tn_t}} \\ {}^b\mathbf{b_{t1}} \times {}^b\mathbf{u_{t1}} & \dots & {}^b\mathbf{b_{tn_t}} \times {}^b\mathbf{u_{tn_t}} \end{bmatrix}}_{\mathbf{A_b}} \mathbf{t} \tag{5}$$

where $\mathbf{A_b}$ is the constant configuration matrix of the embedded actuators. When projecting the wrench in the inertial frame $\mathcal{F}_g$, the wrench matrix $\mathbf{W_t} \in \mathbb{R}^{n \times n_t}$ becomes:

$$\begin{bmatrix} {}^g\mathbf{F_t} \\ {}^g\mathbf{N_t} \end{bmatrix} = \underbrace{\begin{bmatrix} \mathbf{R_{gb}}(\mathbf{x}) & \mathbf{0} \\ \mathbf{0} & \mathbf{R_{gb}}(\mathbf{x}) \end{bmatrix} \mathbf{A_b}}_{\mathbf{W_t}(\mathbf{x})} \mathbf{t} \tag{6}$$

where $\mathbf{R_{gb}}$ is the rotation matrix between $\mathcal{F}_g$ and $\mathcal{F}_b$.

C. End-Effector Dynamics

Based on the Newton-Euler formulation, the dynamic equations of the CDPR driven by UFGs thrusts and elastic cable tensions $[\boldsymbol{\tau}^T, \mathbf{t}^T]^T$ are:

$$\begin{bmatrix} m\mathbb{I} & \mathbf{0} \\ \mathbf{0} & \mathbf{I_g} \end{bmatrix} \begin{bmatrix} \ddot{\mathbf{p}} \\ \dot{\boldsymbol{\omega}} \end{bmatrix} + \begin{bmatrix} \mathbf{0} \\ \boldsymbol{\omega} \times \mathbf{I_g}\boldsymbol{\omega} \end{bmatrix} + \begin{bmatrix} -m\mathbf{g} \\ \mathbf{0} \end{bmatrix} = \begin{bmatrix} \mathbf{W}_\tau & \mathbf{W_t} \end{bmatrix} \begin{bmatrix} \boldsymbol{\tau} \\ \mathbf{t} \end{bmatrix} \tag{7}$$

with $\mathbf{p}$ the coordinates of G, $\boldsymbol{\omega}$ the angular velocity of the end effector in $\mathcal{F}_g$ and $\mathbf{g}$ the gravity vector. The end-effector mass is m, $\mathbf{I_g}(\mathbf{x})$ being its inertia matrix expressed in the inertial frame.

Let $\mathbf{S}(\boldsymbol{\theta})$ be the matrix that links the time derivative of the angular coordinate $\boldsymbol{\theta}$ to the angular velocity $\boldsymbol{\omega}$ [6], such that $\boldsymbol{\omega} = \mathbf{S}(\boldsymbol{\theta})\dot{\boldsymbol{\theta}}$. Substituting $\boldsymbol{\omega}$ in (7) and left-multiplying the rotation dynamics equation by $\mathbf{S^T}$ yields the model of CDPR dynamics :

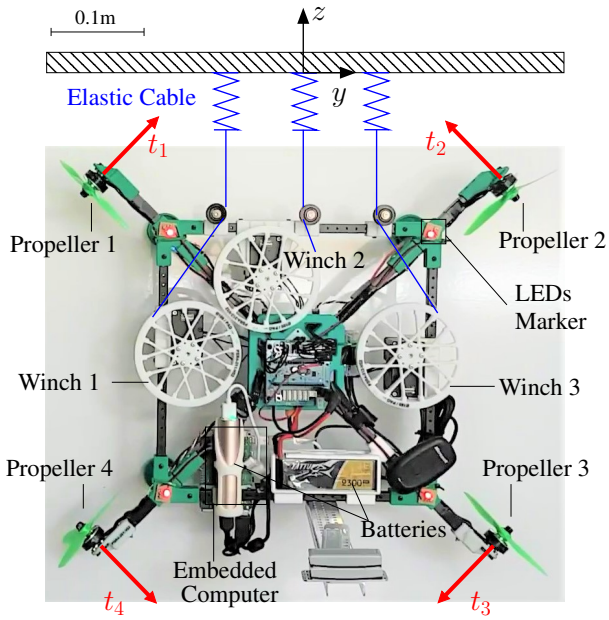

Fig. 2: PiSaRo4 CDPR robot with embedded air propellers.

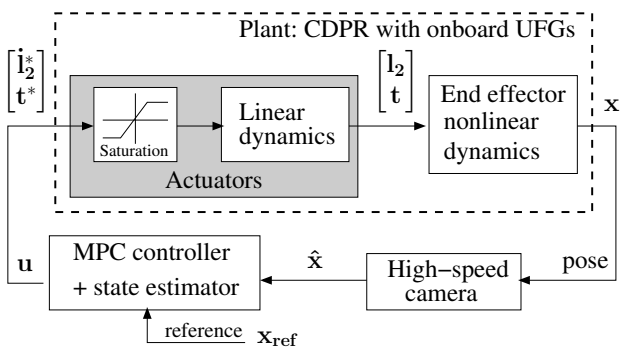

Fig. 3: Constrained MPC control with actuator dynamics.

$$\underbrace{\begin{bmatrix} m\mathbb{I} & \mathbf{0} \\ \mathbf{0} & \mathbf{S}^T\mathbf{I_g}\mathbf{S} \end{bmatrix}}_{\mathbf{M}(\mathbf{x})} \begin{bmatrix} \ddot{\mathbf{p}} \\ \ddot{\boldsymbol{\theta}} \end{bmatrix} + \underbrace{\begin{bmatrix} \mathbf{0} \\ \mathbf{S}^T(\mathbf{I_g}\dot{\mathbf{S}}\dot{\boldsymbol{\theta}} + \mathbf{S}\,\dot{\boldsymbol{\theta}} \times \mathbf{I_g}\mathbf{S}\,\dot{\boldsymbol{\theta}}) \end{bmatrix}}_{\mathbf{C}(\mathbf{x},\dot{\mathbf{x}})\dot{\mathbf{x}}} + \underbrace{\begin{bmatrix} -m\mathbf{g} \\ \mathbf{0} \end{bmatrix}}_{\mathbf{G}} = \underbrace{\begin{bmatrix} \mathbb{I} & \mathbf{0} \\ \mathbf{0} & \mathbf{S}^T \end{bmatrix} \begin{bmatrix} \mathbf{W}_\tau & \mathbf{W_t} \end{bmatrix}}_{\mathbf{W}(\mathbf{x}) \in \mathbb{R}^{n \times (n_t + n_\tau)}} \begin{bmatrix} \boldsymbol{\tau} \\ \mathbf{t} \end{bmatrix} \tag{8a}$$

$$\boldsymbol{\tau} = \mathbf{K}_\tau(\mathbf{l_2})[\mathbf{l_1}(\mathbf{x}) - \mathbf{l_2}] \tag{8b}$$

with the on-board UFG and winch actuator dynamics

$$\begin{bmatrix} \frac{1}{\omega_n^2}\dddot{\mathbf{l}}_\mathbf{2} \\ \mathbf{0} \end{bmatrix} + \begin{bmatrix} \frac{2\xi}{\omega_n}\ddot{\mathbf{l}}_\mathbf{2} \\ T_\tau\dot{\mathbf{t}} \end{bmatrix} + \begin{bmatrix} \dot{\mathbf{l}}_\mathbf{2} \\ \mathbf{t} \end{bmatrix} = \underbrace{\begin{bmatrix} \dot{\mathbf{l}}_\mathbf{2}^* \\ \mathbf{t}^* \end{bmatrix}}_{\mathbf{u}} \tag{9a}$$

$$\text{and input constraint} \begin{bmatrix} -\dot{\mathbf{l}}_\mathbf{2max} \\ \mathbf{t_{min}} \end{bmatrix} \leq \begin{bmatrix} \dot{\mathbf{l}}_\mathbf{2}^* \\ \mathbf{t}^* \end{bmatrix} \leq \begin{bmatrix} \dot{\mathbf{l}}_\mathbf{2max} \\ \mathbf{t_{max}} \end{bmatrix} \tag{9b}$$

III. Experimental Setup

A 3-DoF suspended planar CDPR has been built with redundant actuation using 3 cable winches and 4 propellers. In this study, with a limited loss of generality, the two translational degrees of freedom of the robot suspended by only one cable are considered. The 3 cable ends are attached so that they are parallel (Fig. 2) and the same control signal is sent simultaneously to the three winches resulting in an equivalent single cable CDPR. Note that the rotation around x axis is not controlled yielding free passively damped oscillations of small amplitude.

A. PiSaRo4 Robot

The PiSaRo4 (Fig. 2) has 4 drone propeller UFGs. Since standard electronic speed controllers (ESCs) do not regulate the rotational velocity of the propeller and since the thrust is directly linked to the squared rotational velocity, we implemented an outer fast PID speed regulation loop using real-time ESC telemetry data (source code available at `https://github.com/jacqu/teensyshot`). We tuned the PID controller to achieve a step response shaped like a first order with a $T_\tau = 0.035\,\mathrm{s}$ time constant. The lowest velocity the ESC can regulate is 1250 RPM resulting in a minimum thrust of the propeller $t_{min} = 0.02\,\mathrm{N}$. The maximum thrust is $6.7\,\mathrm{N}$, limited to $t_{max} = 3.8\,\mathrm{N}$ during the experiments for safety reasons. A symmetric location of the propeller [12] has been chosen to maximize the feasible wrench workspace and ensure a null force resultant when the propellers are all running at their lowest speed. The DYNAMIXEL XM540 servomotors are used to drive the winches, yielding a cable winding maximum speed of $\dot{l}_{2max} = 0.26\,\mathrm{m\,s^{-1}}$ and a $100\,\mathrm{ms}$ settling time. Thanks to a carbon-polymer frame, the mass is lowered to $2.55\,\mathrm{kg}$. A spring is inserted between the cable ends and the anchoring points in order to easily emulate the low stiffness of a very long cable in an indoor laboratory environment.

In this work, the position $[y, z]^T$ of the CDPR is measured using a remote $500\,\mathrm{Hz}$ camera acquiring the image of four red LED markers mounted on the end effector. The high level computation and wireless communications are handled by an on-board Raspberry Pi 4 model B computer. Rapid prototyping of the control law is achieved with the RPIt open-source toolbox [19] used with Simulink coder to generate the real-time code running on the on-board computer.

B. PiSaRo4 End-Effector Dynamics

With one equivalent cable and 4 propellers, the PiSaRo4 model can be accurately approximated by a point mass elastic pendulum (Fig. 4). Let $\mathbf{x} = [y, z]^T$ be its pose defined by the position ($z < 0$) of the end-effector center of gravity G in $\mathcal{F}_g$. The stretched cable length is $l_1(\mathbf{x}) = \sqrt{y^2 + z^2}$.

According to the modeling section II, the wrench applied to the end effector is linked to the cable tension by the wrench matrix:

$$\mathbf{W}_\tau = -{}^{\mathbf{g}}\mathbf{u_1} = \begin{bmatrix} -\sin\theta \\ \cos\theta \end{bmatrix} = \frac{1}{\sqrt{y^2 + z^2}} \begin{bmatrix} -y \\ -z \end{bmatrix} \tag{10}$$

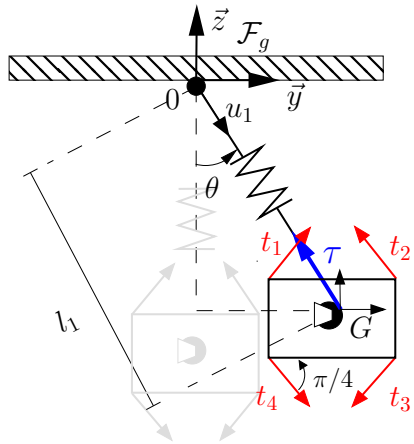

Fig. 4: Elastic pendulum model of the PiSaRo4 robot.

Parameters	m	k_s	f_v	ω_n	ξ	T_τ
Units	kg	N	$\mathrm{N\,m^{-1}\,s}$	$\mathrm{rad\,s^{-1}}$		s
Value	2.55	81	2	32.4	0.78	0.035

TABLE I: PiSaRo4 MODEL PARAMETERS

Similarly, the wrench matrix for the propeller thrusts is:

$$\mathbf{W_t} = \mathbf{A_b} = -\frac{1}{\sqrt{2}}\begin{bmatrix}1 & -1 & -1 & 1\\ 1 & 1 & -1 & -1\end{bmatrix} \tag{11}$$

with $\mathbf{R_{gb}} = \mathbb{I}$, and $\mathbf{A_b}$, the configuration matrix (Eq. (5)) dependent of the mounting of the propellers (Fig. 4).

Finally, from (8a), (10), (11) and the definition of a viscous friction coefficient, f_v, to take into account the weak damping of the system, the CDPR end-effector dynamics equation is:

$$m\begin{bmatrix}\ddot{y}\\ \ddot{z}\end{bmatrix} + f_v\begin{bmatrix}\dot{y}\\ \dot{z}\end{bmatrix} + \begin{bmatrix}0\\ mg\end{bmatrix} = \left[\begin{array}{c|c}\frac{-y}{\sqrt{y^2+z^2}} & \\ \frac{-z}{\sqrt{y^2+z^2}} & \mathbf{A_b}\end{array}\right]\begin{bmatrix}\tau\\ \hline t_1\\ \vdots\\ t_4\end{bmatrix} \tag{12}$$

with $\tau = k(l_2)(\sqrt{y^2+z^2} - l_2)$.

C. Linear Model of the PiSaRo4 with Actuators Saturation

For the following control design, a linear model of the previous dynamics is derived around an equilibrium position $\{y, z\} = \{0, z_0\}$ with $z_0 < 0$.

Let us define z_δ and $l_{2\delta}$, respectively the robot vertical position and the cable free length with respect to the equilibrium state, such that $z_\delta = z - z_0$ and $l_{2\delta} = l_2 - l_{20}$. The cable free length, l_{20}, is fully defined by z_0 at the equilibrium through the static force balance equation: $mg = k(l_{20})[-z_0 - l_{20}]$.

The linear end-effector dynamics (13) in the vicinity of the equilibrium is obtained from a first-order Taylor expansion of (12). These dynamics in y and z coordinates are respectively the dynamics of a pendulum and a mass-spring, which are only coupled by the configuration matrix of the propellers, $\mathbf{A_b}$:

$$m\begin{bmatrix}\ddot{y}\\ \ddot{z_\delta}\end{bmatrix} + f_v\begin{bmatrix}\dot{y}\\ \dot{z_\delta}\end{bmatrix} + k(l_{20})\begin{bmatrix}1+\frac{l_{20}}{z_0}\\ 1\end{bmatrix}\begin{bmatrix}y\\ z_\delta\end{bmatrix} =$$
$$k(l_{20})\begin{bmatrix}0\\ \frac{-z_0}{l_{20}}\end{bmatrix} l_{2\delta} + \underbrace{\frac{1}{\sqrt{2}}\begin{bmatrix}-1 & 1 & 1 & -1\\ -1 & -1 & 1 & 1\end{bmatrix}}_{\mathbf{A_b}}\begin{bmatrix}t_1\\ \vdots\\ t_4\end{bmatrix} \tag{13}$$

with constraints and actuator dynamics given by (9a)-(9b). The saturation and parameter values are given in Table I-II.

IV. Experiments

A. Tuning and Implementation of the MPC Controller

A MPC controller is selected to: i) track a position reference of the CDPR end effector ii) while solving the control allocation, i.e. balancing the contribution of the redundant actuators with respect to their saturation. To meet these objectives, an optimal control input sequence $\mathbf{U} = [\mathbf{u}_0, \ldots, \mathbf{u}_{N-1}]$ is computed, so that the following cost function is minimized under constraints:

$$\min_{\mathbf{U}}\left[\sum_{k=0}^{N-1}\|\mathbf{x_k} - \mathbf{x_{ref}}\|^2_{\mathbf{Q}} + \sum_{k=0}^{N_u-1}\|\mathbf{u_k}\|^2_{\mathbf{R}}\right] \tag{14a}$$

$$\text{s.t.} \quad \mathcal{X}_{\mathbf{k+1}} = \mathbf{A}\mathcal{X}_{\mathbf{k}} + \mathbf{B}\mathbf{u_k},\ \mathbf{x_k} = \mathbf{C}\mathcal{X}_{\mathbf{k}} \tag{14b}$$

$$\begin{bmatrix}-\dot{\mathbf{l}}_{\mathbf{2max}}\\ \mathbf{t_{min}}\end{bmatrix} \le \mathbf{u_k} \le \begin{bmatrix}\dot{\mathbf{l}}_{\mathbf{2max}}\\ \mathbf{t_{max}}\end{bmatrix},\ k = 0, \ldots, N_u - 1 \tag{14c}$$

where:

- $\|x\|^2_{\mathbf{Q}} = x^T\mathbf{Q}x$ and $\mathbf{Q} = \mathrm{diag}(q_{yz}, q_{yz}) \ge 0$, $\mathbf{R} = \mathrm{diag}(r_{l_2}, r_t, r_t, r_t, r_t) > 0$ are two diagonal matrices weighting the tracking error and the control signal energy respectively,
- $\mathbf{x}_{\text{ref}} = [y_{\text{ref}}, z_{\text{ref}}]^T$ is the desired position reference,
- $\mathbf{u}_k = [\dot{l}^*_{2\delta}, t^*_1, t^*_2, t^*_3, t^*_4]^T(k)$ is the input signal of the winch and propeller actuators at sample time k, and $\dot{l}_{2max}$, t_{min}, t_{max} their respective saturation value,
- $\mathcal{X}_k = [y, \dot{y}, z_\delta, \dot{z_\delta}, l_{2\delta}, \dot{l_{2\delta}}, \ddot{l_{2\delta}}, t_1, t_2, t_3, t_4]^T(k)$ is the state vector of a discrete state space representation of the PiSaRo4 with its actuator dynamics, defined by the state, input and output matrices $\{\mathbf{A}, \mathbf{B}, \mathbf{C}\}$.

Since the linear constrained optimization problem is easier to solve and more suitable for real-time applications, using multiple linear models at different operating points is an effective alternative to a nonlinear optimization [20]. Thus, the discrete state equation model (14b) used here is the PiSaRo4 model (13) after discretization at a sampling time T_s =30 ms.

Finally, only the first control input sample $\mathbf{u_0}$ is applied to the system. At the next sampling time, the new position of the end effector is measured by the camera (Fig. 3) and a new constrained optimization is carried out.

For evaluation and comparison, two MPC controllers are tuned: one for the CDPR with winch-only actuation and

MPC	N	N_u	q_{yz}	r_t	r_{i_2}	t_{min}	t_{max}	$\dot{l}_{2max}$
Winch only	40	7	1	-	0.04	-	-	0.26
Winch+Propellers	40	7	1	0.005	0.05	0.02	3.81	0.26

TABLE II: CONTROLLER TUNING PARAMETERS

another for the CDPR with redundant winch and propeller actuation. The size N of the receding horizon is tuned such that NT_s is at least equal to the desired settling time of the closed-loop system. The control signal horizon N_u is usually kept short and smaller than the receding horizon N. The tracking error weight q_{yz} is normalized to 1 and the weights $\{r_{i_2}, r_t\}$ on the winch and thrust control signals are tuned in simulations. Note that the weight r_t has to be kept as small as possible, so that the propellers can significantly contribute to the overall control and improve the system dynamics. However, there is a trade-off: if this weight is too small, the energy of the propellers is not penalized enough, yielding high-power solutions without significant improvement of the robot dynamics. In particular, due to the PiSaRo4 symmetrical configuration of the propellers, any thrust vector $[t_1, t_2, t_3, t_4]^T = \beta[1, 1, 1, 1]^T, \beta \in \mathbb{R}$ results in a null resultant force on the end effector [12] and may be selected if not penalized. All tuning values and input constraints are summarized in Table II.

The MPC controller is implemented on an embedded Raspberry Pi 4 using MATLAB code generation with the Model Predictive Control toolbox.

B. Reference Tracking Experimental Results

A step reference $z_{\delta ref} = 0.1\text{m}$ is used to assess the efficiency of the MPC controller to move the robot from one to another static position with the various actuation strategies. The time response is compared between i) winch only and ii) redundant winch and propeller actuation.

In both cases, the step response is well damped with respect to the lightly damped open loop response as shown in Fig. 5. Saturation constraints on the actuators inputs are respected by the controller: control signals remain within limits represented by horizontal dashed lines. The control signal of each actuator reaches its saturation as expected with an optimal controller. The time response of the winch-only actuation is pretty close to a bang bang solution. The 5% settling time is similar for both strategies, it is only slightly shorter with the winch+propeller compared to the winch-only actuation (see Table III). Note that the settling time from one resting position to another one is limited by the winch maximal velocity. However, the rise time (from 10% to 90%) is reduced by 39% from 0.41 to 0.25s, when the propellers are used simultaneously with winch actuation.

C. Disturbance Rejection Experimental Results

The efficiency of external disturbance rejection using redundant on-board actuators is assessed. These disturbances may result from the wind action in an exterior scenario, a collision with the environment or a gripper releasing its load.

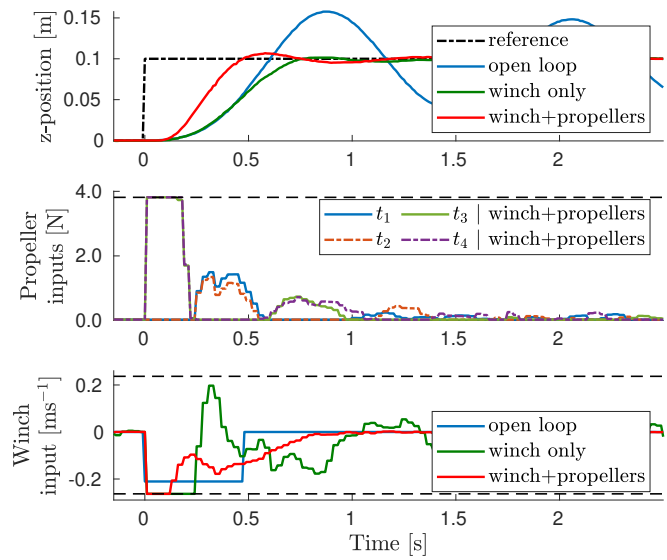

Fig. 5: Step response for a 0.1 meter z-axis reference with i) winch only vs ii) combining winch and propeller actuation.

Actuation	**Settling Time [s]**	**Rise Time [s]**
Winch only	0.70	0.41
Winches + Propellers	0.65(−7 %)	0.25(−39 %)

TABLE III: Z-AXIS REFERENCE TRACKING RESULTS

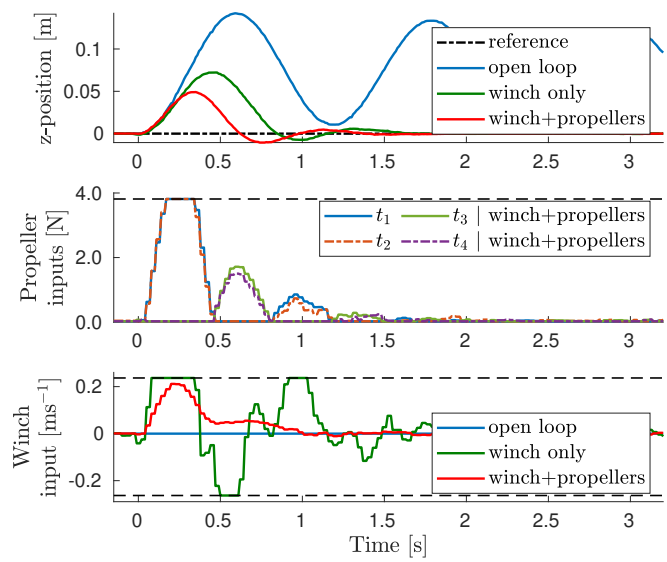

Fig. 6: Step disturbance rejection along z-axis with i) winch only vs ii) combining winch and propeller actuation.

Actuation	**Peak Time [s]**	**Peak Value [m]**
Open loop	0.59	0.142
Winch only	0.47(−20 %)	0.072 (−49 %)
Winch + Propellers	0.35(−40 %)	0.049(−65 %)

TABLE IV: Z-AXIS DISTURBANCE REJECTION RESULTS

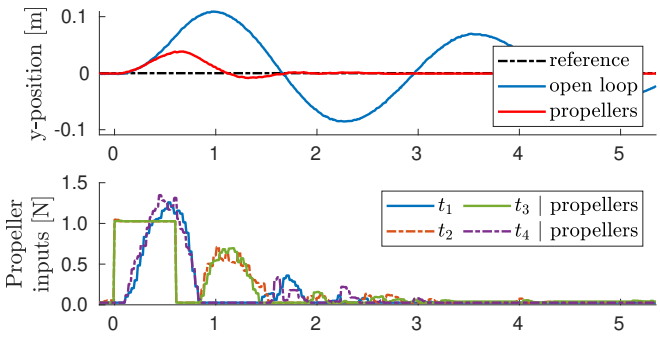

Fig. 7: Step disturbance rejection along y-axis with drone propeller actuation.

Actuation	Peak Time [s]	Peak Value [m]
Open loop	0.98	0.107
Winch + Propellers	0.68(−31 %)	0.038(−64 %)

TABLE V: Y-AXIS DISTURBANCE REJECTION RESULTS

The rejection of a force step disturbance along the z-axis is experimented by cutting a wire holding a $0.75\,\mathrm{kg}$ weight attached to the end effector. The response in Fig. 6 shows that the resulting disturbance is efficiently rejected with the contribution of the propeller actuators. From Table IV, the peak amplitude of the disturbance on the end-effector position is reduced by 32% with respect to the winch-only actuation and by 65% with respect to the open-loop behavior. Moreover, the rejection peak is attained $0.35\,\mathrm{s}$ after the disturbance step with winch+propeller actuation compared to $0.47\,\mathrm{s}$ $(+31\%)$ using winch-only actuation. The winch-only velocity control signal reaches both its upper and lower saturation as expected. However, better rejection is obtained when avoiding saturation of the winch velocity and allowing saturation of the 2 propellers whose thrusts are in the opposite direction of the disturbance.

The rejection of a $0.6\,\mathrm{s}$ impulse disturbance in the y-direction is studied by generating a simultaneous $1\,\mathrm{N}$ thrust on propellers 2 and 3 (Fig. 7). As the winch actuation has no effect in this direction, the winch only or open loop responses have the same lightly damped response. An effective damping of the disturbance is achieved by the MPC control of the propellers with a reduction of 64% of the disturbance amplitude (Table V).

V. Conclusion

In this paper, redundant actuation of a CDPR using high dynamics on-board UFG actuators has been studied. The performance of the proposed MPC control strategy to extend the natural dynamic behavior of a CDPR is assessed experimentally on a planar 2-DoF robot suspended equivalently by 1 cable and actuated by 4 drone propellers. By combining winch and propeller actuation, disturbance rejection is significantly faster and rise time during trajectory tracking is shorter with respect to the winch-only actuation. The MPC controller proves its ability to solve efficiently the control allocation problem by balancing the contribution of each actuator taking into account their respective saturation.

Future work will investigate the performance of nonlinear predictive control for 3-DoF trajectory tracking on the PiSaRo4 robot.

References

[1] P. Tempel, P. Herve, O. Tempier, M. Gouttefarde, and A. Pott, "Estimating inertial parameters of suspended cable-driven parallel robots — use case on cogiro," in *2017 IEEE International Conference on Robotics and Automation (ICRA)*, May 2017, pp. 6093–6098.

[2] D. W. Robinson, J. E. Pratt, D. J. Paluska, and G. A. Pratt, "Series elastic actuator development for a biomimetic walking robot," in *1999 IEEE/ASME International Conference on Advanced Intelligent Mechatronics (Cat. No.99TH8399)*, Sep. 1999, pp. 561–568.

[3] J.-B. Izard, M. Gouttefarde, C. Baradat, D. Culla, and D. Salle, *Integration of a Parallel Cable-Driven Robot on an Existing Building Façade*, 01 2013, vol. 12, pp. 149–164.

[4] R. Thompson and M. Blackstone, "Three-dimensional moving camera assembly with an informational cover housing," Mar. 29 2005, US Patent 6,873,355.

[5] M. A. Khosravi and H. D. Taghirad, "Dynamic modeling and control of parallel robots with elastic cables: Singular perturbation approach," *IEEE Transactions on Robotics*, vol. 30, no. 3, pp. 694–704, June 2014.

[6] J. Begey, L. Cuvillon, M. Lesellier, M. Gouttefarde, and J. Gangloff, "Dynamic control of parallel robots driven by flexible cables and actuated by position-controlled winches," *IEEE Transactions on Robotics*, vol. 35, no. 1, pp. 286–293, 2018.

[7] G. Meunier, B. Boulet, and M. Nahon, "Control of an overactuated cable-driven parallel mechanism for a radio telescope application," *IEEE Transactions on Control Systems Technology*, vol. 17, no. 5, pp. 1043–1054, Sept 2009.

[8] X. Weber, L. Cuvillon, and J. Gangloff, "Active vibration canceling of a cable-driven parallel robot using reaction wheels," in *2014 IEEE/RSJ International Conference on Intelligent Robots and Systems*. IEEE, 2014, pp. 1724–1729.

[9] M. Lesellier, L. Cuvillon, J. Gangloff, and M. Gouttefarde, "An active stabilizer for cable-driven parallel robot vibration damping," in *2018 IEEE/RSJ International Conference on Intelligent Robots and Systems (IROS)*. IEEE, 2018, pp. 5063–5070.

[10] R. de Rijk, M. Rushton, and A. Khajepour, "Out-of-plane vibration control of a planar cable-driven parallel robot," *IEEE/ASME Transactions on Mechatronics*, vol. 23, no. 4, pp. 1684–1692, 2018.

[11] R. Qi, M. Rushton, A. Khajepour, and W. W. Melek, "Decoupled modeling and model predictive control of a hybrid cable-driven robot (hcdr)," *Robotics and Autonomous Systems*, vol. 118, pp. 1–12, 2019.

[12] H. Sellet, I. Khayour, L. Cuvillon, S. Durand, and J. Gangloff, "Active damping of parallel robots driven by flexible cables using cold-gas thrusters," *IEEE International Conference on Robotics and Automation*, 2018.

[13] T. A. Johansen and T. I. Fossen, "Control allocation—a survey," *Automatica*, vol. 49, no. 5, pp. 1087 – 1103, 2013.

[14] J. Guerrero, J. Torres, V. Creuze, and A. Chemori, "Trajectory tracking for autonomous underwater vehicle: An adaptive approach," *Ocean Engineering*, vol. 172, pp. 511–522, Jan. 2019.

[15] Yu Luo, A. Serrani, S. Yurkovich, D. B. Doman, and M. W. Oppenheimer, "Model predictive dynamic control allocation with actuator dynamics," in *Proceedings of the 2004 American Control Conference*, vol. 2, June 2004, pp. 1695–1700 vol.2.

[16] A. Veksler, T. A. Johansen, F. Borrelli, and B. Realfsen, "Dynamic positioning with model predictive control," *IEEE Transactions on Control Systems Technology*, vol. 24, no. 4, pp. 1340–1353, July 2016.

[17] J. M. Maciejowski, *Predictive control: with constraints*. Pearson education, 2002.

[18] M. Gouttefarde, D. Daney, and J.-P. Merlet, "Interval-analysis-based determination of the wrench-feasible workspace of parallel cable-driven robots," *IEEE Transactions on Robotics*, vol. 27, no. 1, pp. 1–13, 2010.

[19] J. Gangloff, A. Yigit, and M. Lesellier, "RPIt," Strasbourg, France, 2019. [Online]. Available: https://github.com/jacqu/RPIt/

[20] A. Bemporad, "Model predictive control design: New trends and tools," in *Proceedings of the 45th IEEE Conference on Decision and Control*. IEEE, 2006, pp. 6678–6683.